Simulation of false-alarm area of laser guidance based on Mie scattering model*

HU Qi-li (胡启立)**, **HUO Jiang-tao** (霍江涛), **MIAO Xi-kui** (苗锡奎), **SHAO Ming** (邵铭), **LI Wu-zhou** (李武周), **and KANG Hua-chao** (康华超)

Key Laboratory of Electro-Optical Countermeasures Test & Evaluation Technology, Luoyang 471003, China

(Received 9 March 2020; Revised 5 July 2020)

In order to study the influence of backscattering of indicating laser in laser guidance process and laser guidance countermeasure test, the scattering function and volume extinction coefficient of typical aerosol distribution are calculated, and the backscattering detection model of 1.06 μm horizontally transmitted laser is established, based on Mie scattering theory and scattering function optimization algorithm; the model is used to study the change of backscattering energy detected by the detector at different positions and different detection angles, and the false-alarm area of laser guidance along the indicating laser path under different detection thresholds is obtained. The results can help to deepen the understanding of the influence of atmospheric scattering on the laser guidance process, and provide theoretical reference for the scheme design of the laser guidance countermeasure test.

Document code: A **Article ID:** 1673-1905(2021)04-0236-5

DOI https://doi.org/10.1007/s11801-021-0041-6

Laser guidance is an effective way of precision guidance and has been widely used and developed, the typical guidance processes are: the laser beam is directed to irradiate the target, and the laser seeker keeps track of the reflected laser signal of the target, so as to finally hit the target accurately[1,2]. In order to improve the guidance accuracy of the guidance system and its adaptability to different environments, for the whole process of laser guidance, researches on the laser reflection characteristics of different target surfaces, the transmission and scattering characteristics of the indicating laser under the atmospheric conditions of raindrops, haze, solid particles, etc., the construction of laser guidance simulation system, the anti-jamming and performance test of the laser seeker have been carried out at home and abroad[3-7].

The above work mainly focuses on the transmission and detection of the indicating laser itself, and the backscattering of the indicating laser has also been studied. The White Sands Missile Range of the United States has established the corresponding test safety rules[8], which are used to avoid the influence of backscattering on the laser guided weapon test; In China, some beneficial theoretical and experimental researches on the backscattering problem in the static erection test and simulation test of laser seeker are also conducted, and the theoretical and experimental results of backscattering detection at a single position have been obtained[9-12]. In this paper, aiming at the typical laser guidance process and atmospheric environment, based on the Mie scattering model, the backscattered light detected by laser seeker in different positions in the area near the indicating laser path is simulated and calculated, and the backscattering distribution received by the detection equipment in the area near the indicating beam is obtained. Due to the diversity and complexity of the actual conditions, this work focuses on theoretical research, but the results can provide references for the subsequent experimental studies of backscattering under different conditions, the design of test scheme, the layout of test positions, etc.

The suspended solid and liquid particles in the atmosphere are called atmospheric aerosols. The number density of aerosol particles changes with the altitude and aerosol scale. In this paper, the aerosol distribution model proposed by McClatchey et al is used[13,14]. As shown in Eq.(1) and Tab.1, the model gives the aerosol size distribution function with normalization parameters c and the vertical distribution of the particle density N under different visibility conditions. After N is determined, the normalized parameters c can be calculated by $N=\int f(r)\mathrm{d}r$, and the distribution functions of aerosol particles spectrum at different altitudes can be obtained as

$$f(r)=\begin{cases} c\times r^{-4}\ (0.1\ \mu\mathrm{m}<r\le 10\ \mu\mathrm{m}) \\ c\times 10^{4}\ (0.02\ \mu\mathrm{m}\le r\le 0.1\ \mu\mathrm{m}) \\ 0\ (r<0.02\ \mu\mathrm{m}, r>10\ \mu\mathrm{m}) \end{cases}. \tag{1}$$

* This work has been supported by the Fund for Key Laboratory of Electro-Optical Countermeasures Test & Evaluation Technology (No.GKCP2019001).

** E-mail: husmail@163.com

Tab.1 The vertical distribution of the particle density

Altitude (km)	Particle density N (particles/cm^3)	
	23 km visibility	5 km visibility
0	2 828	13 780
1	1 224	5 030
2	537.1	1 884
3	225.6	673.1
4	119.2	245.3

For example, when the atmospheric visibility is 5 km, the particle density at the ground is N=13 780, and the normalized results is c=12.158 8. The aerosol size distribution function at the ground can be obtained by Eq.(1).

Under the assumption that the aerosol particles are homogeneous and spherical, the Mie scattering light field of a single particle can be accurately solved by solving Maxwell equation. If the electric field intensity of incident plane wave is $\boldsymbol{E}$ and the magnetic field intensity is $\boldsymbol{H}$, then the radiation flux density or average energy flux density of incident light field in the air medium is

$$\boldsymbol{S}_{\mathrm{av}} = \frac{1}{2}\mathrm{Re}[\boldsymbol{E}\times\boldsymbol{H}] = \frac{1}{2}\sqrt{\frac{\varepsilon}{\mu}}\left|E_0\right|^2\boldsymbol{e}_z , \tag{2}$$

where $\boldsymbol{e}_z$ is the unit vector determined by the right-hand spiral rule, that is, the incident light intensity is $I_0 = \frac{1}{2}\sqrt{\frac{\varepsilon}{\mu}}\left|\boldsymbol{E}_0\right|^2$, and then the scattered light intensity is

$$I = \frac{I_0\lambda^2}{4\pi^2 l^2}F(\beta,\varphi)(\theta\in[0,\pi],\varphi\in[0,2\pi]) , \tag{3}$$

where l is the distance from the scattering center to the observation point, λ is the incident light wavelength, β is the scattering angle, φ is the angle between the incident plane and the scattering plane, $F(\beta, \varphi)$ is called Mie scattering function. When the incident light is un-polarized, the scattering function can be expressed as[10,15]: $F(\beta, \varphi) = [|S_1(\beta)|^2 + |S_2(\beta)|^2]/2$, where $S_1(\beta)$ and $S_2(\beta)$ are the scattering amplitude functions, which are independent of φ and can be calculated as

$$S_1(\beta) = \sum_{n=1}^{\infty}\frac{2n+1}{n(n+1)}(a_n\pi_n + b_n\tau_n) , \tag{4}$$

$$S_2(\beta) = \sum_{n=1}^{\infty}\frac{2n+1}{n(n+1)}(a_n\tau_n + b_n\pi_n) , \tag{5}$$

where π_n and τ_n are scattering angle functions, and the calculation equations are as follow:

$$\begin{cases}\pi_n = \dfrac{2n-1}{n-1}\cos\beta\times\pi_{n-1} - \dfrac{n}{n-1}\pi_{n-2}\\ \tau_n = n\cos\beta\times\pi_n - (n+1)\pi_{n-1}\\ \pi_0 = 0\\ \pi_1 = 1\end{cases} , \tag{6}$$

a_n and b_n are Mie scattering coefficients, and the calculation equations are:

$$a_n = \frac{\phi_n(\alpha)\phi_n'(m\alpha) - m\phi_n'(\alpha)\phi_n(m\alpha)}{\xi_n(\alpha)\phi_n'(m\alpha) - m\xi_n'(\alpha)\phi_n(m\alpha)} , \tag{7}$$

$$b_n = \frac{m\phi_n(\alpha)\phi_n'(m\alpha) - \phi_n'(\alpha)\phi_n(m\alpha)}{m\xi_n(\alpha)\phi_n'(m\alpha) - \xi_n'(\alpha)\phi_n(m\alpha)} , \tag{8}$$

where m is the refractive index of aerosol particles and $\alpha=2\pi r/\lambda$ is the dimensionless parameter related to the size of aerosol particles. ϕ_n and ξ_n are Riccati-Bessel functions, and the solutions require to calculate the first and second kind of semi-odd order Bessel functions directly[16,17]. When α or the imaginary part of m are relatively large, the high order term of Bessel function will lead to slow calculation or overflow of calculation results. Shen Jianqi decomposes a_n and b_n into new recursive terms by deforming the above formula, as shown in Eq.(9), which can effectively avoid the phenomenon that the data caused by the calculation of Bessel function alone is too large and then overflows[18].

$$\begin{cases}a_n = A_n(\alpha)\times T_{a_n}(m,\alpha)\\ b_n = A_n(\alpha)\times T_{b_n}(m,\alpha)\end{cases} , \tag{9}$$

where

$$\begin{cases}T_{a_n}(m,\alpha) = \dfrac{D_n(m\alpha)/m - D_n(\alpha)}{D_n(m\alpha)/m - B_n(\alpha)}\\ T_{b_n}(m,\alpha) = \dfrac{mD_n(m\alpha) - D_n(\alpha)}{mD_n(m\alpha) - B_n(\alpha)}\\ A_n(\alpha) = \phi_n(\alpha)/\xi_n(\alpha)\\ B_n(\alpha) = \xi_n'(\alpha)/\xi_n(\alpha)\\ D_n(\alpha) = \phi_n'(\alpha)/\phi_n(\alpha)\end{cases} . \tag{10}$$

The recurrence relations are

$$\begin{cases}A_n(\alpha) = A_{n-1}(\alpha)\dfrac{B_n(\alpha)+n/\alpha}{D_n(\alpha)+n/\alpha}\\ B_n(\alpha) = -n/\alpha + \dfrac{1}{n/\alpha - B_{n-1}(\alpha)}\\ D_{n-1}(\alpha) = n/\alpha - \dfrac{1}{n/\alpha + D_n(\alpha)}\end{cases} . \tag{11}$$

The initial conditions are

$$\begin{cases}A_0(\alpha) = \dfrac{1}{1+\mathrm{i}\dfrac{\cos\alpha}{\sin\alpha}}\\ B_0(\alpha) = -\mathrm{i}\end{cases} . \tag{12}$$

In order to improve the calculation accuracy, according to Eq.(10), the back recurrence method is used to calculate the value of each D_n, but the first recurrence term D_N is calculated by Lentz continued fraction[19,20]. The number of cut-off terms N is twice of the calculation result of empirical formula $\alpha+7.5\alpha^{1/3}+2$[18], and the maximum number of different cut-off terms corresponding to different α is taken to ensure the accuracy of calculation.

When m=1.33, the angle distribution diagram of Mie scattering function under different scale parameter α is drawn. It can be seen from Fig.1 that when α is small, the

forward scattering and backward scattering are almost the same. With the increase of α, the scattered light gradually concentrates in the front. By observing the image of scattering intensity magnified by 100 times as shown in the dotted line within the range of 90°—270° in the right figure of Fig.1, it can be seen that when α is large, the back scattering intensity fluctuates greatly with the scattering angle.

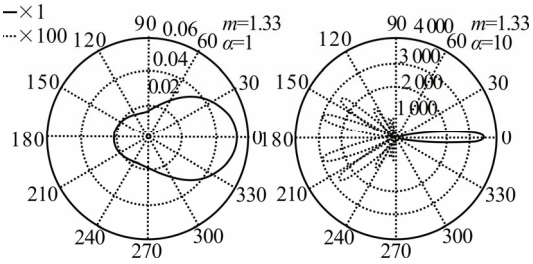

Fig.1 Angle distribution of Mie scattering function under different α

The calculation accuracy of Mie scattering function can be verified by calculating extinction efficiency factor Q_{ext} and scattering efficiency factor Q_{sca}[15]. The calculation results of the particles with different scale parameters and refractive indices are shown in Tab.2, which are consistent with those calculated by MIECPP method[21] in different refractive index and large scale range. The accuracy of the results is mainly related to recurrence method, calculation accuracy setting, selection of cut-off terms, etc.

Tab.2 Results of Q_{ext} and Q_{sca}[21]

m	α	Q_{ext}	Q_{sca}
0.75	0.099	$7.417\,86\times10^{-6}$	$7.417\,86\times10^{-6}$
1.33×10^{-5}i	10 000	2.004 09	1.723 86
1.5−i	0.055	0.101 491	$1.131\,69\times10^{-5}$
1.5−i	100	2.097 50	1.283 70
10−10i	10 000	2.005 91	1.795 39

In order to establish the detection model of the backscattering of the indicating laser, it is advisable to set the indicating laser to transmit horizontally at the ground level. The detector is located near the indicating beam and can receive the backscattering of the indicating beam. The spatial position relationship of the detection model is shown in Fig.2, indicating laser is emitted from the laser source S and transmitted along the horizontal light path, the diameter of the beam at the exit is D_0, the energy of the single pulse is Q_0, the pulse width is t_0, and the beam divergence angle is θ; the horizontal distance between the target T and S is R, the off-axis distance of the detector D is h, the horizontal distance of the detector D is L, and the angles between DS, DT and optical path are δ_1 and δ_2, respectively; the field angle of the detector is V_ϕ, the angle between the lower edge of the field of view and the horizontal direction is α_{V1} and it intersects with the optical axis at F_1, the angle between the upper edge of the field of view and the horizontal direction is α_{V2} and it intersects with the optical axis at F_2; the distance between S and the scattering point F in the field of view is y and the scattering angle is β, the angle between the scattered light and the optical axis of the detection field of view is γ (not shown in Fig.2).

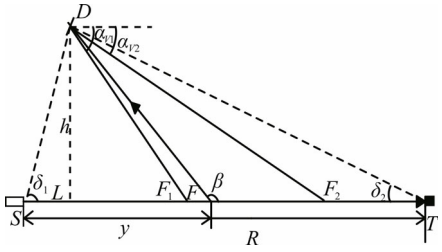

Fig.2 Sketch map of backscattering detection of indicating laser

According to Eq.(3) and the attenuation law of laser propagation in the atmosphere[11,13], the backscattered laser energy density of aerosol particles in volume element $S_y\mathrm{d}y$ at position F detected by detector D is as follows:

$$\mathrm{d}W_s(y)=\frac{Q_0}{(D_0+\theta y)^2/4}\exp(-\tau(y+\sqrt{h^2+(y-L)^2}))\times\int_{r}\frac{F(\beta,\alpha)\cos\gamma f(r)\mathrm{d}r}{k^2(h^2+(y-L)^2)}\pi\frac{(D_0+\theta y)^2}{4}\mathrm{d}y. \quad (13)$$

After simplification, we get:

$$\mathrm{d}W_s(y)=Q_0\exp(-\tau(y+\sqrt{h^2+(y-L)^2}))\times\frac{\pi}{(h^2+(y-L)^2)}\int_{r_1}^{r_2}\frac{F(\beta,\alpha)\cos\gamma}{k^2}f(r)\mathrm{d}r\mathrm{d}y, \quad (14)$$

where $k=2\pi/\lambda$, τ is the extinction coefficient. When only considering the extinction caused by Mie scattering, τ is equal to Mie scattering extinction coefficient τ_{ext}. According to $\tau_{\text{ext}}=\pi\int_{r_1}^{r_2}r^2f(r)Q_{\text{ext}}\mathrm{d}r$, τ_{ext}[15,20] can be obtained, and the unit of τ_{ext} can be converted into km^{-1}. For 1.06 μm laser, under the condition of m=1.33 and V=5 km, τ_{ext}=0.281 km^{-1} can be calculated. At this time, according to formula $I/I_0=\exp(-\tau_{\text{ext}}L)$, the laser energy at the position 5km away from S decreases by 75.5%.

Without considering the influence of the diffuse reflection light, by integrating the scattering volume elements in the field of view along the optical path ST, the total energy density of scattered light detected by the detector is $W_s=\int_{y_1}^{y_2}\mathrm{d}W_s(y)$, y_1 and y_2 are the distances from S to F_1 and F_2 respectively. Polar coordinate system is established in DST plane, with detector D as the pole, horizontal direction as the polar axis and clockwise direction as positive. Suppose that the deflection angle

between the optical axis direction of the detector field of view and the horizontal direction is ϕ_0, then the deflection angle between the lower edge DF_1 of the field of view and the horizontal direction is $\alpha_{V1}=\phi_0+V_\phi/2$, the deflection angle between the upper edge DF_2 of the field of view and the horizontal direction is $\alpha_{V2}=\phi_0-V_\phi/2$, the deflection angle between the laser source S and the detector D is $\delta_S=\pi-\delta_1=\pi-\text{actg}(h/L)$, and the deflection angle between the target T and the detector D is:

$$\delta_T=\delta_2=\text{arctg}(\frac{h}{R-L}). \tag{15}$$

For different situations, y_1 and y_2 have different values. When $\delta_S>\alpha_{V1}>\delta_T>\alpha_{V2}$, there are:

$$\begin{cases} y_1=\text{ctg}\alpha_{V1}\times h+L \\ y_2=R \end{cases}. \tag{16}$$

When $\delta_S>\alpha_{V1}>\alpha_{V2}>\delta_T$, there are:

$$\begin{cases} y_1=\text{ctg}\alpha_{V1}\times h+L \\ y_2=\text{ctg}\alpha_{V2}\times h+L \end{cases}. \tag{17}$$

In the above cases, the scattered light from y_1 to y_2 enters the detector's field of view. When the scattering signal strength W_S detected by the detector exceeds the detector's detection threshold, the scattering signal can cause false alarm interference to the detector.

According to the calculation process of Mie scattering model and backscattering detection model, the specific parameters are set as follow: laser wavelength λ=1.06μm, spot diameter at the light outlet D_0=1 cm, beam divergence angle θ=1 mrad, visibility V=5 km, target distance R=9 km, detector field of view V_ϕ=20°, aerosol particle refractive index m=1.33, and the aerosol particle size distribution at the ground is represented by Eq.(1).

By changing the deflection angle ϕ_0, when L=0 km, at different h, the curves of scattering intensity W_S with ϕ_0 show a similar trend. As shown in Fig.3, W_S first fluctuates and increases, then decreases rapidly, and there is an approximate peak position on each curve.

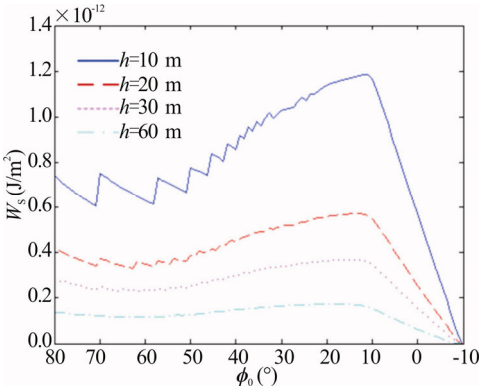

Fig.3 Energy density detected as a function of detection angle (*L*=0 km)

The factors leading to the change of W_S are the change of scattering angle, the change of the length of the scattering beam in the detection field of view and the attenuation of laser energy: when the ϕ_0 decreases from 80°, the length of the scattering beam in the field of view increases, the laser energy decays, and the scattering coefficient fluctuates with the scattering angle, the path increment plays an important role in the change of W_S, and the detection energy curve shows a fluctuating and rising trend; when the ϕ_0 is reduced to 10°, that is, the target T is in the field of view, with the decrease of ϕ_0, the length of the scattering beam in the field of view is shortened, at the same time, the laser energy attenuation increases, and the detected scattering energy drops rapidly, affected by these factors, the detection energy curve reaches the peak value near 10° after the fluctuation and rise; when the detection angle is in the range of 30°—80°, the detection energy curve will fluctuate, and when the detection angle is less than 10°, the detection energy curve will decline smoothly, this change trend of detection energy curve is mainly affected by the change of backscattering with angle, that is, the total backscattering of particle ensemble has different change trends in different angle ranges, and when the scattering angle is close to the incident optical axis, the total backscattering keeps a smooth trend with the change of scattering angle.

It can be seen from Fig.3 that the detected scattering energy fluctuates greatly with the change of detection angle ϕ_0, and when ϕ_0 is different there is no uniform trend of the detected scattering energy with the change of h. However, when observing the change of maximum detection energy with h, a series of curves of the maximum detected energy density varying with h are obtained as shown in Fig.4. It can be found that the detection energy peak decreases smoothly with the increase of h, and when L is different, the different curves are approximately distributed. With the increase of L, the maximum detection energy density corresponding to h decreases, and the curve also tends to be flat.

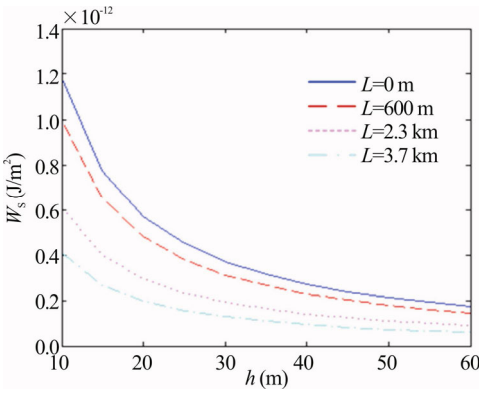

Fig.4 Energy density detected as a function of detection height

By observing the change of maximum detection energy with h and L, the spatial distribution curves of detection energy density in the area near the indicating laser path are obtained as shown in Fig.5.

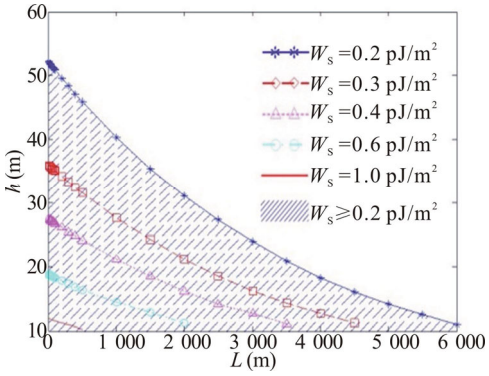

Fig.5 The spatial distribution curves of detection energy density and section of the false-alarm area

The spatial distribution curves of detection energy density show similar changes, and the detection energy decreases smoothly with the increase of off-axis distance h and horizontal distance L; taking the spatial distribution curves as the generatrices, the spatial distribution surfaces of the detection energy density can be formed, and the surfaces can form approximate cone areas, when the threshold value of detector is lower than the detection energy corresponding to a certain surface, the detector in the corresponding cone area can be interfered by the back scattering light of the indicating beam, the area is the false alarm area of detector; when the threshold value of the detector decreases, the boundary of the false alarm area expands outwards, that is, the false alarm area gradually expands with the decrease of the threshold value of the detector.

The above results are calculated under the condition that each model parameter is fixed. Because the laser guidance process or laser countermeasure test is affected by aerosol distribution, target direction, target distance, indicating laser parameter, detector field of view, detector sensitivity and other factors, the next step, different conditions will be set to study the influence of the above factors on the laser guidance false alarm area, and experimental verification will also be carried out.

The Mie scattering function and the atmospheric extinction coefficient of single Mie scattering are calculated based on the Mie scattering model of laser atmospheric transmission. On this basis, a detection model of backscattering of indicating laser is established, the variation of detection energy with detection direction and detector position is analyzed and studied, and the spatial distribution of the false alarm area near the light path is obtained. The laser seeker and other detection equipment in the area are vulnerable to the interference of backscattering, the area distribution is affected by the aerosol distribution, target distance, indicating laser parameters, detector field of view and detector sensitivity. The research results are helpful to deepen the understanding of the influence of atmospheric scattering on the laser guidance process, and provide a theoretical reference for the scheme design of the laser guidance countermeasure test.

References

[1] Chen Cheng, Zhao Liang-yu and Ma Xiao-ping, Laser & Infrared **49**, 131 (2019). (in Chinese)

[2] Qiu Xiong, Liu Zhi-guo and Wang Shi-cheng, Chinese Journal of Lasers **46**, 57 (2019). (in Chinese)

[3] Liu Dan, Laser Scattering Characteristics of Radar Stations in Complex Environment, Xi'an: Xidian University, 1 (2018). (in Chinese)

[4] Li Kui, Study on the Light Scattering Characteristics of Targets on the Sea Surface, Xi'an: Xidian University, 1 (2018). (in Chinese)

[5] Zhang Su, Zhan Jun-tong, Fu Qiang, Duan Jin, Li Ying-chao and Jiang Hui-lin, Acta Optica Sinica **39**, 0629001-1 (2019). (in Chinese)

[6] Pu Xiao-qin, Dong Quan-lin and Du Ya-wen, Electronic Test **23**, 67 (2018). (in Chinese)

[7] Liu Ke-jian, Miao Xi-kui, Xu Chen-yang, Wang Ye, Zhang Jun-qiang, Yang Bin and Sun Ting-ting, Chinese Journal of Optics **12**, 257 (2019). (in Chinese)

[8] Range Commanders Council, Laser Range Safety, New Mexico: White Sands Missile Range, 316-98 (1998).

[9] Li Hua, Key Techniques Research on Laser Guidance Information Fields Simulation, Changsha: National University of Defense Technology, 1 (2010). (in Chinese)

[10] Yao Mei, Zhang Le, Li Ying-hua and Hu Xin, Infrared and Laser Engineering **36**, 385 (2007). (in Chinese)

[11] Zhang Yan-xiu, Wang Zhi-qing, Liu Li-wu, Liang Dongming and Xu Tian-ye, Modern Electronics Technique **35**, 38 (2012). (in Chinese)

[12] Liu Hui, Gu Qiong-qiong, Li Ying-bo and Xie Yuan-hua, Guidance & Fuze **39**, 1 (2018). (in Chinese)

[13] Li Jing-zhen, Handbook of Optics, Xi'an: Shanxi Science and Technology Press, 1752 (2010). (in Chinese)

[14] McClatchey R A, Optical Properties of the Atmosphere, Massachusetts: Air Force Camb. Res. Lab., 108 (1971).

[15] McCartney E J, Optics of the Atmosphere: Scattering by Molecules and Particles, Beijing: Science Press, 1988.

[16] Rao Rui-zhong, Modern Atmospheric Optics, Beijing: Science Press, 219 (2012). (in Chinese)

[17] Milton Abramowitz, Handbook of Mathematical Functions with Fomulas, Graphs, and Mathematical Tables, Washington D.C.: U. S. Government Printing Office, 437 (1970).

[18] Shen Jian-qi and Liu Lei, China Powder Science and Technology **11**, 45 (2005). (in Chinese)

[19] Lentz W J, Applied Optics **15**, 668 (1976).

[20] Wu De-huai, Research on Fast Algorithm for MIE Scattering Coefficients in Wide Range, Xi'an: Xi'an University of Electronic Science and Technology, 22 (2009). (in Chinese)

[21] Hong Du, Applied Optics **43**, 1951 (2004).